BNL-NUREG -29047
INFORMAL REPORT
LIMITED DISTRIBUTION

ANALYSIS OF THE ORNL POOL CRITICAL ASSEMBLY PRESSURE VESSEL DOSIMETRY BENCHMARK EXPERIMENT

D. K. MIN, A. ARONSON AND J. F. CAREW

DATE PUBLISHED - FEBRUARY 1981

CORE PERFORMANCE GROUP

DEPARTMENT OF NUCLEAR ENERGY BROOKHAVEN NATIONAL LABORATORY
UPTON, NEW YORK 11973

Prepared for the U.S. Nuclear Regulatory Commission
Office of Nuclear Reactor Regulation
Contract No. DE-AC02-76CH00016

NOTICE

BNL-NUREG-29047
INFORMAL REPORT
LIMITED DISTRIBUTION

ANALYSIS OF THE ORNL POOL CRITICAL ASSEMBLY PRESSURE VESSEL DOSIMETRY BENCHMARK EXPERIMENT

D. K. Min[†], A. Aronson and J. F. Carew

Draft Report Completed - January 1981
Date Published - February 1981

Core Performance Group
Department of Nuclear Energy
Brookhaven National Laboratory
Upton, New York 11973

Prepared for
U.S. Nuclear Regulatory Commission
Washington, D. C. 20555
Under Interagency Agreement DE-AC02-76CH00016
NRC FIN No. A-3126

[†] Visiting IAEA Fellow, Korea Nuclear Fuel Development Institute

ABSTRACT

In order to evaluate dosimetry methods used to determine pressure vessel damage fluence, the Oak Ridge Pool Critical Assembly (PCA) Pressure Vessel Dosimetry Benchmark Experiment has been calculated. One-hundred group ENDF/B-IV cross sections were collapsed to sixteen groups for each PCA material zone using ANISN, and a two-dimensional DOT 3.5 neutron flux calculation performed. The calculations were performed in an S_8P_3 approximation in a fixed source mode. The measured foil $^{27}AL(n,\alpha)$, $^{56}Fe(n,p)$, $^{32}S(n,p)$, $^{58}Ni(n,p)$, $^{115}In(n,n')$, $^{237}Np(n,f)$ and $^{238}U(n,f)$ activations were determined using ENDF/B-V cross sections and the calculated neutron flux. The calculations were found to under predict the activation measurements by $\sim$ 5-10% for energies above 1 MeV and by $\sim$ 10-20% for energies above .1 MeV.

TABLE OF CONTENTS

LIST OF FIGURES

LIST OF TABLES

I. INTRODUCTION

As part of the Division of Systems Integration Radiation Embrittlement Program and in order to confirm the dosimetry methods of BNL and other evaluators, the Oak Ridge National Laboratory (ORNL) Pool Critical Assembly (PCA) Pressure Vessel Dosimetry Benchmark Experiment[1] has been calculated. One-dimensional and two-dimensional models of the ORNL PCA-Pressure Vessel Facility were set up and calculated using the ANISN[2] and DOT 3.5[3] discrete ordinate transport codes. The 100-neutron group EPR[4] cross section set was used to construct a collapsed 16-neutron group material dependent cross section library. A flow chart of the BNL calculational scheme is presented in Figure 1.

Comparison with the PCA measurements indicates the calculations are 5-10% low for energies above 1 MeV and $\sim$ 10 - 20% low at energies above .1MeV. These differences are believed to be due to three-dimensional effects not included in the calculations.

II. EXPERIMENT

The basic components of the PCA are the PCA core, window simulator, thermal shield, pressure vessel simulator and void box. The PCA core consists of 4 different fuel elements, i.e., standard 18-plate fuel elements (fuel type 1), 17-plate fuel elements (fuel type 2), 9-plate control elements (fuel type 3) and 19-plate fuel elements (fuel type 4). The fuel loading pattern is given in Figure 2.

The components outside of the core which are of primary importance are the thermal shield and the pressure vessel simulator. The thermal shield is fabricated from type 304L stainless steel, and the pressure vessel simulator is composed of type SA-36 carbon steel.

The compositions and number densities of the basic components of the PCA are given in Tables 1a and 1b.

The foil measurement locations (A1 through A8) for the PCA 8/7 and PCA 12/13 configuration are given in Figure 3 and Figure 4. The most important measurement locations are the A4, A5 and A6 locations which are the 1/4, 1/2 and 3/4 pressure vessel thickness locations.

III. CALCULATIONS

Nuclear Data

The neutron transport cross sections used in all of the calculations were based on the ENDF/B-IV 100-neutron group EPR library[4] distributed by RSIC at ORNL. The foil activations were determined using the ENDF/B-V 100-group

dosimetry cross sections for $^{27}Al(n,\alpha)$, $^{56}Fe(n,p)$, $^{32}S(n,p)$, $^{58}Ni(n,p)$, $^{115}In(n,n')$, $^{237}Np(n,f)$, $^{197}Au(n,\gamma)$, $^{232}Th(n,f)$, $^{235}U(n,f)$ and $^{238}U(n,f)$. The $^{103}Rh(n,n')$ $^{103}Rh^{m}$ cross section was not available in ENDF/B-V, and was obtained from D. C. Santry and J. P. Bulter's measurements.[5]

The ENDF/B-V U-235 Watt fission spectrum was used in all calculations including the spectral averaging of the dosimetry cross sections necessary for the determination of the equivalent fission flux.

Spatially Dependent Cross Sections

In order to generate cell weighted cross sections, one-dimensional ANISN models for each fuel type were set up and are presented in Table 2. The 100-group EPR cross sections were collapsed to 16-groups and homogenized by cell flux weighting and in Table 3 the 16-group structure and corresponding EPR groups are given. Sixteen-group material dependent cross sections for each zone given in Table 4 and Table 5 were also determined.

One-Dimensional Calculations

The one-dimensional geometry models of the PCA 8/7 and 12/13 configuration are given in Table 4 and Table 5. There are 98 mesh intervals for the PCA 8/7 and 108 mesh intervals for the PCA 12/13 configuration.

The radial power distribution at the mid-plane included in the technical letter for the PCA Blind Test[1] was used to determine the source. The fixed source as a function of radial mesh interval in each group was obtained by multiplying the relative power at each mesh interval by the U-235 fission spectrum. The neutron source over the full core was normalized to one neutron/sec.

Both one-dimensional 100-group and 16-group ANISN models were calculated. All calculations were performed in a fixed source mode, P3 transport cross section expansion and S8 angular quadrature using ANISN. The core regions were assumed to be a homogenized Uranium-Water-Aluminum mixture. The left boundary was treated as the axis of symmetry using a reflective boundary condition.

A comparison of the 100-group and 16-group ANISN fluxes was performed to determine the adequacy of the 16-group structure. The results are given in table 6 and indicate this group structure reproduces the 100-group flux above .1MeV to within < 3% at the measurement locations.

Two-Dimensional Calculations

The two-dimensional DOT 3.5 geometry models of the PCA 12/13 and PCA 8/7 configuration are given in Figure 5 and Figure 6. There are (108, 20) and (98, 20) mesh intervals for the PCA 12/13 and 8/7 configurations respectively.

The power distribution for the two-dimensional DOT (x,y) calculations was determined from the power distribution included in the Technical Letter for PCA Blind Test[2] using linear interpolation and is given in Figure 7. The fixed source was obtained as a product of power distribution at the center of each mesh interval in the core multiplied by the U-235 fission spectrum.

The neutron source over the full core was normalized to one neutron/sec., i.e.,

$$2\Sigma s(x,y)\Delta x\Delta y \cdot 2 \cdot 1.019 \int_{-30}^{30} \cos\,(0.044\,(z + 4.42))\,dz \qquad (1)$$

$$= 1 \text{ neutron/sec}$$

or,

$$\Sigma s(x,y)\Delta x\Delta y = 5.67884 \times 10^{-3} \text{ neutron/cm} \qquad (2)$$

where s(x,y) is the spatial source.

The two-dimensional DOT(x,y) calculations were performed using the collapsed 16-group neutron cross sections. A P3 scattering cross section and a fully symmetric S8 angular quadrature set (48 angles) were used. The left and bottom boundaries in the two-dimensional calculations were treated as axes of symmetry with reflective boundary conditions. And the right and top boundaries were treated with vacuum boundary conditions. Quarter core symmetry was assumed. The fuel regions were considered as spatially uniform regions for which the cross sections were collapsed and spatially homogenized as described above.

A comparison of DOT(x,y) fluxes with a pointwise convergence of EPS = 0.3×10^{-2} and 0.5×10^{-3} was performed and the results given in Table 7 indicate the flux has converged.

Leakage Correction

In order to account for axial effects that are not included in the DOT(x,y) model, one-dimensional ANISN(x) and two-dimensional DOT(x,z) calculations were performed using the 16-group cross section set for the PCA 12/13 and PCA 8/7 configurations. The DOT(x,z) calculational models for the PCA 12/13 and PCA 8/7 configuration are given in Figure 8 and Figure 9.

Axial correction factors for the measurement locations in each group were determined by dividing the DOT(x,z) flux by the corresponding ANISN(x) flux.

The three-dimensional flux in group g, $\phi_g(x,y,z)$, was then obtained by multiplying the DOT(x,y) flux in group g, $\phi_g^{DOT}(x,y)$, by the axial correction factor in group g, LFg(z),

$$\phi_g(x,y,z) = \phi_g^{DOT}(x,y) * \frac{\phi_g^{DOT}(x,z)}{\phi_g^{ANISN}(x)} = \phi_g^{DOT}(x,y) * LFg(z) \quad (3)$$

Reaction Rate and Equivalent Fission Flux

The reaction rates for each reaction type and measurement location were calculated using $\phi_g(x,y,z)$ and the 16-group dosimetry cross sections. The dosimetry cross sections were collapsed to 16-groups using 100-group ANISN fluxes determined for each measurement location.

In order to reduce the dependence of the calculated reaction rates on the dosimetry cross sections, equivalent fission fluxes were defined as the absolute reaction rates divided by the average dosimetry cross section in a "pure" U-235 fission field. The average dosimetry cross sections in a pure U-235 fission field were calculated and are given in Table 12.

IV. RESULTS AND DISCUSSION

Groupwise axial correction factors for the PCA 12/13 and PCA 8/7 configuration are given in Table 8 and Table 9 and indicate the axial correction is larger at lower energy as expected. The groupwise neutron flux for the PCA 12/13 and PCA 8/7 configuration is given in Table 10 and Table 11. The reaction rate and equivalent fission flux for each reaction type and location are given in Tables 12-15.

The calculated and measured equivalent fission fluxes for the PCA 12/13 and PCA 8/7 configurations are compared in Table 16 and Table 17. The calculation/measurement differences range from 0 to -30% for the 24 measured activations with the differences generally increasing as the reaction threshold decreases and the measured flux decreases in energy. It is seen that the equivalent fission flux at the A6 location for $^{27}Al(n,\alpha)$, which has the highest threshold energy (5.0 MeV), is $\sim$ 6-8% lower than the measurement value, whereas the equivalent fission flux for $^{237}Np(n,f)$ and $^{103}Rh(n,n')$, which have the lowest threshold energy (0.1 MeV), is $\sim$ 20% lower than the measurement value. However, the $^{238}U(n,f)$ reaction has an intermediate threshold of 0.7 MeV and shows the largest difference. This inconsistency may be due to measurement error.

The axial leakage correction, calculated as the ratio of the two-dimensional DOT(x,z) flux to the one-dimensional ANISN(x) flux, is known to overestimate the axial effect, especially in the lower energy groups, and is believed responsible for the increase in the calculation/measurement differences for the low threshold activations.

REFERENCES

1. Letter, F. B. K. Kam to distribution, "Technical Letter for PCA Blind Test," June, 1977.

2. W. W. Engle, Jr., "A User's Manual for the ANISN code," USAEC Report K-1693, Oak Ridge Gaseous Diffusion Plant (1967)

3. "DOT 3.5 - A Two-Dimensional Discrete Ordinates Transport Code," CCC-276 (1975), Distributed by the ORNL Radiation Shielding Information Center.

4. W. E. Ford III, R. T. Sanford, R. W. Roussin and D. M. Plaster, "Modification Number One to the 100 n-21γ Cross Section Library," ORNL/TM-5249, Mar. (1976): Available as DLC-37D/EPR RSIC, ORNL.

5. D. C. Santry and J. P. Butler, "Cross Section Measurements for the $^{103}Rh(n,n')\ ^{103}Rh^{m}$ Reaction from 0.122 to 14.74 MeV," Can. J. Phys. 52, 1421 (1974).

TABLE 1a MATERIAL NUMBER DENSITIES [Atoms/Barn-cm]

	^{235}U	^{238}U	Al	H	O
Fuel Type 1					
1. Fuel Plate Meat	8.4758(-4)	6.2991(-5)	4.8499(-2)		
2. Clad			6.0244(-2)		
3. Water			8.6362(-3)	5.8936(-2)	2.9468(-2)
Fuel Type 2					
1. Fuel Plate Meat	8.5133(-4)	6.3269(-5)	4.8494(-2)		
2. Clad			6.0244(-2)		
3. Water			8.4037(-3)	5.9029(-2)	2.9515(-2)
Fuel Type 3					
1. Fuel Plate Meat	8.4971(-4)	6.3149(-5)	4.8496(-2)		
2. Clad			6.0244(-2)		
3. Water			1.2986(-2)	5.2933(-2)	2.6467(-2)
Fuel Type 4					
1. Fuel Plate Meat	1.1592(-3)	8.6147(-5)	4.8086(-2)		
2. Clad			6.0244(-2)		
3. Water			8.3199(-3)	5.9274(-2)	2.9637(-2)

TABLE 1b MATERIAL NUMBER DENSITIES Atoms/Barn-cm

Material Zone	Al	H	O	Mn	Si	Cr	Ni	C	Fe
1. Coolant		6.6464(-2)	3.3232(-2)						
2. Al-Window	6.0244(-2)								
3. Thermal Shield				1.7540(-3)	1.7155(-3)	1.7606(-2)	8.2064(-3)	1.2037(-4)	5.8665(-2)
4. Pressure Vessel								9.8558(-4)	8.4440(-2)

TABLE 2. One-Dimensional Model for the Core Fuel Assemblies

	Thickness (cm)	Mesh
Fuel Type 1 (18 Plates)		
1. Fuel Meat	0.0254	6
2. Clad	0.0508	6
3. Water	0.1488	8
Fuel Type 2 (17 Plates)		
1. Fuel Meat	0.0254	6
2. Clad	0.0508	6
3. Water	0.1620	8
Fuel Type 3 (9 Plates)		
1. Fuel Meat	0.0254	6
2. Clad	0.0508	6
3. Water	0.3738	8
Fuel Type 4 (19 Plates)		
1. Fuel Meat	0.0254	6
2. Clad	0.0381	6
3. Water	0.1497	8

TABLE 3. 16 - Group Energy Structure

Group	EPR[+] Group	Energy (ev)	Fission Spectrum
1	1 - 11	1.4918(7) - 4.9659(6)[++]	5.7375(-2)
2	12 - 16	4.9659(6) - 3.0119(6)	1.5022(-1)
3	17 - 18	3.0119(6) - 2.4660(6)	8.4800(-2)
4	19	2.4660(6) - 2.2313(6)	4.5210(-2)
5	20 - 21	2.2313(6) - 1.8268(6)	9.2250(-2)
6	22 - 26	1.8268(6) - 1.1080(6)	2.1265(-1)
7	27 - 33	1.1080(6) - 5.5023(5)	1.9935(-1)
8	34 - 49	5.5023(5) - 1.1109(5)	1.4074(-1)
9	50 - 63	1.1109(5) - 3.3546(3)	1.7313(-2)
10	64 - 70	3.3546(3) - 5.8295(2)	8.8954(-5)
11	71 - 77	5.8295(2) - 1.0130(2)	6.4525(-6)
12	78 - 82	1.0130(2) - 2.9023(1)	4.2669(-7)
13	83 - 91	2.9023(1) - 3.0590(0)	7.4649(-8)
14	92 - 95	3.0590(0) - 1.1254(0)	2.0547(-9)
15	96 - 99	1.1254(0) - 4.1400(-1)	3.1130(-10)
16	100	4.1400(-1)- 1.0000(-4)	0.0

[+]DLC-37D/EPR(RSIC)
[++]Read as 4.9659 x10^6

TABLE 4. ANISN One-Dimensional Model for the PCA 12/13 Configuration

		Thickness (cm)	Mesh
1.	Core	20.25	15
2.	Water	0.5	2
3.	Aluminum Window	2.5	5
4.	Water	12.3	21
5.	Thermal Shield (SS-304L)	5.9	12
6.	Water	12.8	18
7.	Pressure Vessel (Carbone Steel)	22.5	26
8.	Aluminum Wall	0.3175	2
9.	Void Box (Air)	30.145	3
10.	Aluminum Wall	0.3175	2
11.	Water	7.77	2

TABLE 5. ANISN One-Dimensional Model for the PCA 8/7 Configuration

	Thickness (cm)	Mesh
1. Core	20.25	15
2. Water	0.5	2
3. Aluminum Window	2.5	5
4. Water	8.4	16
5. Thermal Shield (SS-304L)	5.9	12
6. Water	6.7	13
7. Pressure Vessel (Carbone Steel)	22.5	26
8. Aluminum Wall	0.3175	2
9. Void Box (Air)	30.145	3
10. Aluminum Wall	0.3175	2
11. Water	7.77	2

TABLE 6. Comparison of ANISN 100 and 16 Group Fluxes

	Location						
Group	A0	A1	A2	A3	A4	A5	A6
1	1.00+	0.99	0.99	0.98	0.98	0.97	0.96
2	1.00	0.99	0.99	0.97	0.96	0.96	0.96
3	1.00	1.00	0.99	0.99	0.98	0.97	0.97
4	1.00	1.00	0.99	1.00	0.98	0.97	0.96
5	1.00	1.00	0.99	0.99	0.98	0.99	0.99
6	1.00	0.99	0.99	0.97	0.97	0.98	0.99
7	1.00	1.00	0.99	0.99	0.98	1.01	1.01
8	1.00	0.99	0.98	0.99	1.00	0.99	0.99
9	1.00	0.97	0.97	1.00	1.15	1.17	1.10
10	1.00	0.99	0.97	0.99	1.06	1.14	1.14
11	1.00	0.99	0.97	0.99	1.06	1.18	1.16
12	1.00	1.00	0.97	0.99	1.03	1.11	1.12
13	1.00	1.00	0.97	0.99	1.01	1.02	1.02
14	1.00	1.00	0.97	0.99	1.01	1.02	1.02
15	1.00	1.00	0.97	0.99	1.00	1.01	1.00
16	1.00	1.00	0.97	0.98	0.98	1.03	0.96
ϕ>1.0MeV	1.00	0.99	0.99	0.98	0.97	0.98	0.98
ϕ>0.1MeV	1.00	0.99	0.99	0.98	0.99	0.99	0.99

+ $\frac{\text{ANISN 16 GP FLUX}}{\text{ANISN 100 GP FLUX}}$

TABLE 7. Comparison of DOT(x,y) Fluxes for Pointwise Convergence of $\varepsilon=0.3\times10^{-2}$ and $\varepsilon=0.5\times10^{-3}$

	Location						
Group	A0	A1	A2	A3	A4	A5	A6
1	1.00[+]	1.00	1.00	1.00	1.00	1.00	1.00
2	1.00	1.00	1.00	1.00	1.00	1.00	1.00
3	1.00	1.00	1.00	1.00	1.00	1.00	1.00
4	1.00	1.00	1.00	1.00	1.00	1.00	1.00
5	1.00	1.00	1.00	1.00	1.00	1.00	1.00
6	1.00	1.00	1.00	1.00	1.00	1.00	1.00
7	1.00	1.00	1.00	1.00	1.00	1.00	1.00
8	1.00	1.00	1.00	1.00	1.00	1.00	1.00
9	1.00	1.00	1.00	1.00	1.01	1.01	1.01
10	1.00	1.00	1.00	1.00	1.01	1.01	1.01
11	1.00	1.00	1.00	1.00	1.01	1.01	1.01
12	1.00	1.00	1.00	1.00	1.01	1.01	1.01
13	1.00	1.00	1.00	1.00	1.01	1.01	1.01
14	1.00	1.00	1.00	1.00	1.00	1.01	0.99
15	1.00	1.00	1.00	1.00	1.00	1.00	1.00
16	1.00	1.00	1.00	1.03	1.01	1.01	0.98
ϕ>1.0MeV	1.00	1.00	1.00	1.00	1.00	1.00	1.00
ϕ>0.1MeV	1.00	1.00	1.00	1.00	1.00	1.00	1.00

[+] $\dfrac{\text{FLUX}\ (E=0.3\times10^{-2})}{\text{FLUX}\ (E=0.5\times10^{-5})}$

TABLE 8. Groupwise Flux Axial Correction Factor for the PCA 12/13 Configuration.

	Location						
Group	A0	A1	A2	A3	A4	A5	A6
1	1.00	0.83	0.77	0.74	0.71	0.69	0.68
2	1.01	0.85	0.80	0.76	0.73	0.71	0.70
3	1.01	0.86	0.80	0.77	0.73	0.71	0.70
4	1.00	0.86	0.80	0.77	0.73	0.71	0.70
5	1.01	0.87	0.81	0.77	0.73	0.71	0.69
6	1.02	0.87	0.81	0.77	0.72	0.70	0.68
7	1.00	0.87	0.81	0.77	0.70	0.70	0.65
8	1.01	0.88	0.81	0.77	0.67	0.64	0.61
9	1.00	0.88	0.81	0.77	0.67	0.63	0.60
10	0.99	0.88	0.81	0.77	0.68	0.63	0.56
11	0.98	0.88	0.81	0.79	0.69	0.63	0.53
12	0.98	0.88	0.81	0.77	0.69	0.63	0.53
13	0.97	0.88	0.81	0.77	0.70	0.64	0.52
14	0.97	0.88	0.81	0.77	0.70	0.64	0.51
15	0.97	0.88	0.81	0.77	0.71	0.65	0.49
16	0.94	0.85	0.79	0.78	0.76	0.71	0.39
ϕ >1.0MeV	1.01	0.86	0.80	0.76	0.72	0.71	0.69
ϕ >0.1MeV	1.01	0.87	0.80	0.76	0.69	0.66	0.63

TABLE 9. Groupwise Flux Axial Correction Factor for the PCA 8/7 Configuration.

	Location						
Group	A0	A1	A2	A3	A4	A5	A6
1	1.00	0.86	0.80	0.79	0.76	0.74	0.73
2	1.01	0.89	0.82	0.82	0.78	0.76	0.74
3	1.01	0.89	0.82	0.82	0.78	0.76	0.74
4	1.00	0.89	0.82	0.82	0.78	0.76	0.74
5	1.01	0.89	0.83	0.82	0.78	0.76	0.74
6	1.01	0.90	0.83	0.82	0.77	0.75	0.73
7	1.01	0.90	0.83	0.82	0.74	0.71	0.69
8	1.01	0.90	0.82	0.81	0.71	0.68	0.65
9	1.00	0.91	0.82	0.81	0.71	0.67	0.63
10	0.99	0.91	0.82	0.81	0.72	0.67	0.60
11	0.98	0.91	0.82	0.81	0.74	0.68	0.58
12	0.98	0.91	0.82	0.81	0.74	0.68	0.57
13	0.97	0.91	0.82	0.81	0.75	0.69	0.57
14	0.97	0.91	0.82	0.81	0.75	0.69	0.56
15	0.97	0.91	0.82	0.81	0.76	0.70	0.54
16	0.94	0.87	0.80	0.80	0.79	0.73	0.42
ϕ>1.0MeV	1.01	0.89	0.82	0.82	0.77	0.75	0.73
ϕ>0.1MeV	1.01	0.89	0.82	0.81	0.73	0.70	0.66

TABLE 10. Neutron Flux for the PCA 12/13 Configuration
(Axial Correction Applied)

Group	Location A0	A1	A2	A3	A4	A5	A6
1	1.29786+(-5)	3.93117(-7)	4.60261(-8)	1.86800(-8)	3.68939(-9)	1.31593(-9)	4.58315(-10)
2	3.35283(-5)	7.51717(-7)	7.36257(-8)	2.50431(-8)	4.76251(-9)	1.68650(-9)	5.86281(-10)
3	2.10651(-5)	4.70832(-7)	4.71031(-8)	1.50124(-8)	3.54464(-9)	1.34731(-9)	4.94425(-10)
4	1.18412(-5)	2.83501(-7)	3.00453(-8)	9.41117(-9)	2.68654(-9)	1.08859(-9)	4.20830(-10)
5	2.14012(-5)	4.24162(-7)	4.60607(-8)	1.36166(-8)	4.72542(-9)	2.02600(-9)	8.15838(-10)
6	5.49340(-5)	1.03516(-7)	1.25641(-7)	3.29336(-8)	1.63086(-8)	8.27508(-9)	3.81761(-9)
7	6.49651(-5)	1.17547(-6)	1.13964(-7)	3.84618(-8)	3.20343(-8)	2.12471(-8)	1.22680(-8)
8	8.38107(-5)	1.63885(-6)	2.38554(-7)	5.57267(-8)	5.87550(-8)	4.52105(-8)	2.81909(-8)
9	8.69923(-5)	1.94157(-6)	2.84967(-7)	6.89600(-8)	5.57016(-8)	4.36224(-8)	2.61123(-8)
10	3.60280(-5)	9.00635(-7)	1.25812(-7)	3.10708(-8)	9.34294(-9)	5.67595(-9)	3.05899(-9)
11	3.48090(-5)	9.33566(-7)	1.26767(-7)	3.32473(-8)	7.94720(-9)	3.99782(-9)	1.91429(-9)
12	2.41388(-5)	6.89765(-7)	9.14371(-8)	2.36463(-8)	6.32603(-9)	3.02409(-9)	1.36003(-9)
13	4.15921(-5)	1.29354(-6)	1.66172(-7)	4.43460(-8)	1.02047(-8)	4.54598(-9)	1.91917(-9)
14	1.80471(-5)	5.94532(-7)	7.41710(-8)	2.02197(-8)	3.11538(-9)	1.25948(-9)	5.10278(-10)
15	1.75228(-5)	6.05549(-7)	7.39905(-8)	2.05446(-8)	1.95089(-9)	6.59977(-10)	2.52077(-10)
16	3.15474(-4)	6.93630(-5)	3.61466(-6)	1.98659(-6)	1.42315(-8)	7.89506(-10)	2.30607(-10)
ϕ>1.0MeV	1.68327(-4)	3.58609(-6)	3.90569(-7)	1.22144(-7)	4.19198(-8)	1.98534(-8)	8.96873(-9)
ϕ>0.1MeV	3.13487(-4)	6.37286(-6)	8.00381(-7)	2.15990(-7)	1.32245(-7)	8.66915(-8)	4.97426(-8)

TABLE 11. Neutron Flux for the PCA 8/7 Configuration

(Axial Correction Applied)

Group	Location A0	A1	A2	A3	A4	A5	A6
1	1.30248+(-5)	7.27787(-7)	7.93814(-8)	6.82878(-8)	1.37863(-8)	4.86727(-9)	1.69202(-9)
2	3.37457(-5)	1.55012(-6)	1.42678(-7)	1.19218(-7)	2.36896(-8)	8.20890(-9)	2.80716(-9)
3	2.12362(-5)	9.87628(-7)	9.54424(-8)	7.93638(-8)	1.92831(-8)	7.14309(-9)	2.57131(-9)
4	1.19646(-5)	5.97660(-7)	6.19703(-8)	5.17383(-8)	1.50382(-8)	5.93999(-9)	2.25470(-9)
5	2.17471(-5)	9.29001(-7)	9.75762(-8)	8.07407(-8)	2.71355(-8)	1.12402(-8)	4.41505(-9)
6	5.56064(-5)	2.34513(-6)	2.73979(-7)	2.22362(-7)	1.00304(-7)	4.89714(-8)	2.20252(-8)
7	6.65330(-5)	2.76402(-6)	3.69632(-7)	2.95262(-7)	2.12864(-7)	1.36381(-7)	7.72895(-8)
8	8.52282(-5)	3.93417(-6)	5.55729(-7)	4.51181(-7)	4.08195(-7)	3.02208(-7)	1.84822(-7)
9	8.86843(-5)	4.76549(-6)	6.85706(-7)	5.70700(-7)	4.10063(-7)	3.06507(-7)	1.78954(-7)
10	3.68134(-5)	2.23699(-6)	3.06594(-7)	2.56666(-7)	7.63699(-8)	4.41142(-8)	2.29857(-8)
11	3.56068(-5)	2.33896(-6)	3.10558(-7)	2.62322(-7)	6.78041(-8)	3.27218(-8)	1.50443(-8)
12	2.47102(-5)	1.73999(-6)	2.25400(-7)	1.91379(-7)	5.46014(-8)	2.52433(-8)	1.09152(-8)
13	4.26200(-5)	3.28904(-6)	4.13285(-7)	3.53091(-7)	8.91948(-8)	3.86972(-8)	1.57082(-8)
14	1.85056(-5)	1.51709(-6)	1.85311(-7)	1.58892(-7)	2.75922(-8)	1.09021(-8)	4.24455(-9)
15	1.79745(-5)	1.54786(-6)	1.85541(-7)	1.59544(-7)	1.73743(-8)	5.76481(-9)	2.10343(-9)
16	3.21239(-4)	1.08438(-4)	6.90264(-6)	6.17939(-6)	6.36847(-8)	4.21201(-9)	1.60204(-9)
ϕ>1.0MeV	1.70208(-4)	7.67251(-6)	8.22598(-7)	6.78882(-7)	2.40452(-7)	1.12778(-7)	5.07308(-8)
ϕ>0.1MeV	3.18223(-4)	1.43265(-5)	1.74704(-6)	1.42695(-6)	8.62545(-7)	5.56540(-7)	3.16315(-7)

TABLE 12. Dosimeter Reaction Rates for the PCA 12/13 Configuration

Reaction	σ(barns)	Location A1	A2	A3	A4	A5	A6
$^{27}Al(n,\alpha)$	8.12126+(-4)	6.45094(-9)	8.69220(-10)	3.79393(-10)	8.25411(-11)	3.15274(-11)	1.17482(-11)
$^{56}Fe(n,p)$	1.10967(-3)	8.35469(-9)	1.07104(-9)	4.55702(-10)	9.60704(-11)	3.58780(-11)	1.30828(-11)
^{32}S (n,p)	6.35522(-2)	3.59912(-7)	3.80947(-8)	1.38122(-8)	2.82274(-9)	1.02510(-9)	3.63530(-10)
$^{58}ni(n,p)$	1.01150(-1)	5.81543(-7)	6.21274(-8)	2.25542(-8)	4.70794(-9)	1.73144(-9)	6.21962(-10)
$^{115}In(n,n')$	1.73129(-1)	9.19370(-7)	9.93934(-8)	3.16518(-8)	9.15850(-9)	3.98281(-9)	1.66996(-9)
$^{237}Np(n,f)$	1.32546(0)	8.28611(-6)	9.05054(-7)	2.77066(-7)	1.04444(-7)	5.60707(-8)	2.82162(-8)
$^{197}Au(n,\gamma)$	1.71424(-1)	7.86484(-3)	5.53473(-4)	2.35447(-4)	1.63746(-5)	8.21337(-6)	4.09731(-6)
$^{232}Th(n,f)$	7.26637(-2)	3.98485(-7)	4.32714(-8)	1.45280(-8)	3.72299(-9)	1.50465(-9)	5.85941(-10)
^{235}U (n,f)	1.23831(0)	3.52536(-2)	1.85046(-3)	1.01067(-3)	8.58315(-6)	1.09845(-6)	4.53784(-7)
^{238}U (n,f)	2.94208(-1)	1.58329(-6)	1.70995(-7)	5.62614(-8)	1.49630(-8)	6.13678(-9)	2.42136(-9)
$^{103}Rh(n,n')$	7.17704(-1)	3.88758(-6)	4.43010(-7)	1.34383(-2)	5.01541(-8)	2.57761(-8)	1.25741(-8)

* Average Cross section Weighted with a U-235 Fission Spectrum.

TABLE 13. Dosimeter Reaction Rates for the PCA 8/7 Configuration

Reaction	Location A1	A2	A3	A4	A5	A6
$^{27}Al(n,\alpha)$	1.13783+(-8)	1.43706(-9)	1.25114(-9)	2.77001(-10)	1.04704(-10)	3.90153(-11)
$^{56}Fe(n,p)$	1.49947(-8)	1.79648(-9)	1.55724(-9)	3.34111(-10)	1.23384(-10)	4.49245(-11)
^{32}S (n,p)	7.16752(-7)	7.12026(-8)	6.01103(-8)	1.27999(-8)	4.57903(-9)	1.60958(-9)
$^{58}Ni(n,p)$	1.15556(-6)	1.15980(-7)	9.79406(-8)	2.14083(-8)	7.78806(-9)	2.78397(-9)
$^{115}In(n,n')$	1.93574(-6)	2.00203(-7)	1.66166(-7)	5.02248(-8)	2.16414(-8)	9.03648(-9)
$^{237}Np(n,f)$	1.74562(-5)	1.89211(-6)	1.55999(-6)	6.31374(-7)	3.36478(-7)	1.68635(-7)
$^{197}Au(n,\gamma)$	1.39817(-2)	1.18595(-3)	1.03367(-3)	1.33033(-4)	6.58896(-5)	3.15574(-5)
$^{232}Th(n,f)$	8.22548(-7)	8.48679(-8)	7.09825(-8)	1.90999(-8)	7.63937(-9)	2.95652(-9)
^{235}U (n,f)	5.52798(-2)	3.54620(-3)	3.17220(-3)	4.37383(-5)	7.67048(-6)	3.35819(-6)
^{238}U (n,f)	3.29436(-6)	3.38926(-7)	2.82716(-7)	7.85763(-8)	3.18072(-8)	1.24446(-8)
$^{103}Rh(n,n')$	8.32988(-6)	9.11909(-7)	7.51104(-7)	2.93593(-7)	1.50768(-7)	7.36451(-8)

TABLE 14. Equivalent Fission Fluxes for the PCA 12/13 Configuration

	Location					
	A1	A2	A3	A4	A5	A6
Reaction						
$^{27}Al(n,\alpha)$	7.94327+(-6)	1.07030(-6)	4.67160(-7)	1.01636(-7)	3.88208(-8)	1.44660(-8)
$^{56}Fe(n,p)$	7.52900(-6)	9.65188(-7)	4.10664(-7)	8.65756(-8)	3.23321(-8)	1.17898(-8)
$^{32}S\ (n,p)$	5.66325(-6)	5.99424(-7)	2.17336(-7)	4.44161(-8)	1.61300(-8)	5.72018(-9)
$^{58}Ni(n,p)$	5.74931(-6)	6.14211(-7)	2.22978(-7)	4.65441(-8)	1.71175(-8)	6.14891(-9)
$^{115}In(n,n')$	5.31032(-6)	5.74100(-7)	1.82822(-7)	5.28999(-8)	2.30049(-8)	9.64576(-9)
$^{237}Np(n,f)$	6.25150(-6)	6.82823(-7)	2.09034(-7)	7.87983(-8)	4.22953(-8)	2.12879(-8)
$^{197}Au(n,\gamma)$	4.58795(-2)	3.22868(-3)	1.37348(-3)	9.55210(-5)	4.79126(-5)	2.39016(-5)
$^{232}Th(n,f)$	5.48396(-6)	5.95502(-7)	1.99935(-7)	5.12359(-8)	2.07070(-8)	8.06374(-9)
$^{235}U(n,f)$	2.84691(-2)	1.49434(-3)	8.16169(-4)	6.93134(-6)	8.87056(-7)	3.66454(-7)
$^{238}U(n,f)$	5.38153(-6)	5.81204(-7)	1.91230(-7)	5.08586(-8)	2.08586(-8)	8.23010(-9)
$^{103}Rh(n,n')$	5.41668(-6)	6.17260(-7)	1.87239(-7)	6.98813(-8)	3.59146(-8)	1.75199(-8)

TABLE 15. Equivalent Fission Flux for the PCA 8/7 Configuration

Reaction	Location A1	A2	A3	A4	A5	A6
$^{27}Al(n,\alpha)$	1.40105+(-5)	1.76950(-6)	1.54057(-6)	3.41081(-7)	1.28926(-7)	4.80409(-8)
$^{56}Fe(n,p)$	1.35128(-5)	1.61893(-6)	1.40336(-6)	3.01090(-7)	1.11190(-7)	4.04846(-8)
^{32}S (n,p)	1.12782(-5)	1.12038(-6)	9.45841(-7)	2.01408(-7)	7.20515(-8)	2.53270(-8)
$^{58}Ni(n,p)$	1.14242(-5)	1.14661(-6)	9.68271(-7)	2.11649(-7)	7.69952(-8)	2.75232(-8)
$^{115}In(n,n')$	1.11809(-5)	1.15638(-6)	9.59781(-7)	2.90100(-7)	1.25002(-7)	5.21951(-8)
237Np(n,f)	1.31699(-5)	1.45751(-6)	1.17694(-6)	4.76343(-7)	2.53858(-7)	1.27228(-7)
$^{197}Au(n,\gamma)$	8.15621(-2)	6.91823(-3)	6.02990(-3)	7.76047(-4)	3.84366(-4)	1.84090(-4)
$^{232}Th(n,f)$	1.13199(-5)	1.16795(-6)	9.76863(-7)	2.62853(-7)	1.05133(-7)	4.06877(-8)
$^{235}U(n,f)$	4.46413(-2)	2.86374(-3)	2.56172(-3)	2.53210(-5)	6.19431(-6)	1.71191(-6)
$^{238}U(n,f)$	1.11974(-5)	1.15199(-6)	9.60939(-7)	2.67077(-7)	1.08112(-7)	4.22986(-8)
$^{103}Rh(n,n')$	1.13444(-5)	1.27059(-6)	1.04654(-6)	4.09073(-7)	2.10069(-7)	1.02612(-7)

TABLE 16. Comparison of Calculated and Measured Equivalent Fission Flux for the PCA 12/13 Configuration

Reaction	Threshold Energy (MeV)	Calculated/Measured A1	A2	A3	A4	A5	A6
$^{27}Al(n,\alpha)$	5.9	1.02	--	--	1.00	0.95	0.94
$^{56}Fe(n,p)$	5.0	--	--	--	--	--	--
^{32}S (n,p)	1.6	--	--	--	--	--	--
$^{58}Ni(n,p)$	1.0	1.01	--	--	0.90	0.84	0.84
$^{115}In(n,n')$	.42	0.97	--	--	0.91	0.85	0.83
$^{237}Np(n,f)$	.10	0.97	--	--	0.85	0.83	0.80
$^{197}Au(n,\gamma)$	Intermediate	--	--	--	--	--	--
$^{232}Th(n,f)$	.8	--	--	--	--	--	--
^{235}U (n,f)	Thermal	--	--	--	--	--	--
^{238}U (n,f)	.7	--	--	--	0.81	0.76	0.72
$^{103}Rh(n,n')$	.1	1.00	--	--	0.91	0.88	0.84

-- Measurement not available

TABLE 17. Comparison of Calculated and Measured Equivalent Fission Flux for the PCA 8/7 Configuration

Reaction	Threshold Energy (MeV)	Calculated/Measured A1	A2	A3	A4	A5	A6
$^{27}Al(n,\alpha)$	5.9	--	--	--	0.95	0.91	0.92
$^{56}Fe(n,p)$	5.0	--	--	--	--	--	--
^{32}S (n,p)	1.6	--	--	--	--	--	--
$^{58}Ni(n,p)$	1.1	--	--	--	0.88	0.82	0.81
$^{115}In(n,n')$	0.4	--	--	--	0.86	0.79	0.74
$^{237}Np(n,f)$	0.1	0.93	--	--	0.82	0.79	0.75
$^{197}Au(n,\gamma)$	Intermediate	--	--	--	--	--	--
$^{232}Th(n,f)$	0.8	--	--	--	--	--	--
^{235}U (n,f)	Thermal	--	--	--	--	--	--
^{238}U (n,f)	0.7	--	--	--	0.79	0.74	0.69
$^{103}Rh(n,n')$	0.1	--	--	--	0.87	0.83	0.79

-- Measurement not available

FIGURE 1 Flow Chart of PCA Pressure Vessel Dosimetry Benchmark Experiment Calculations

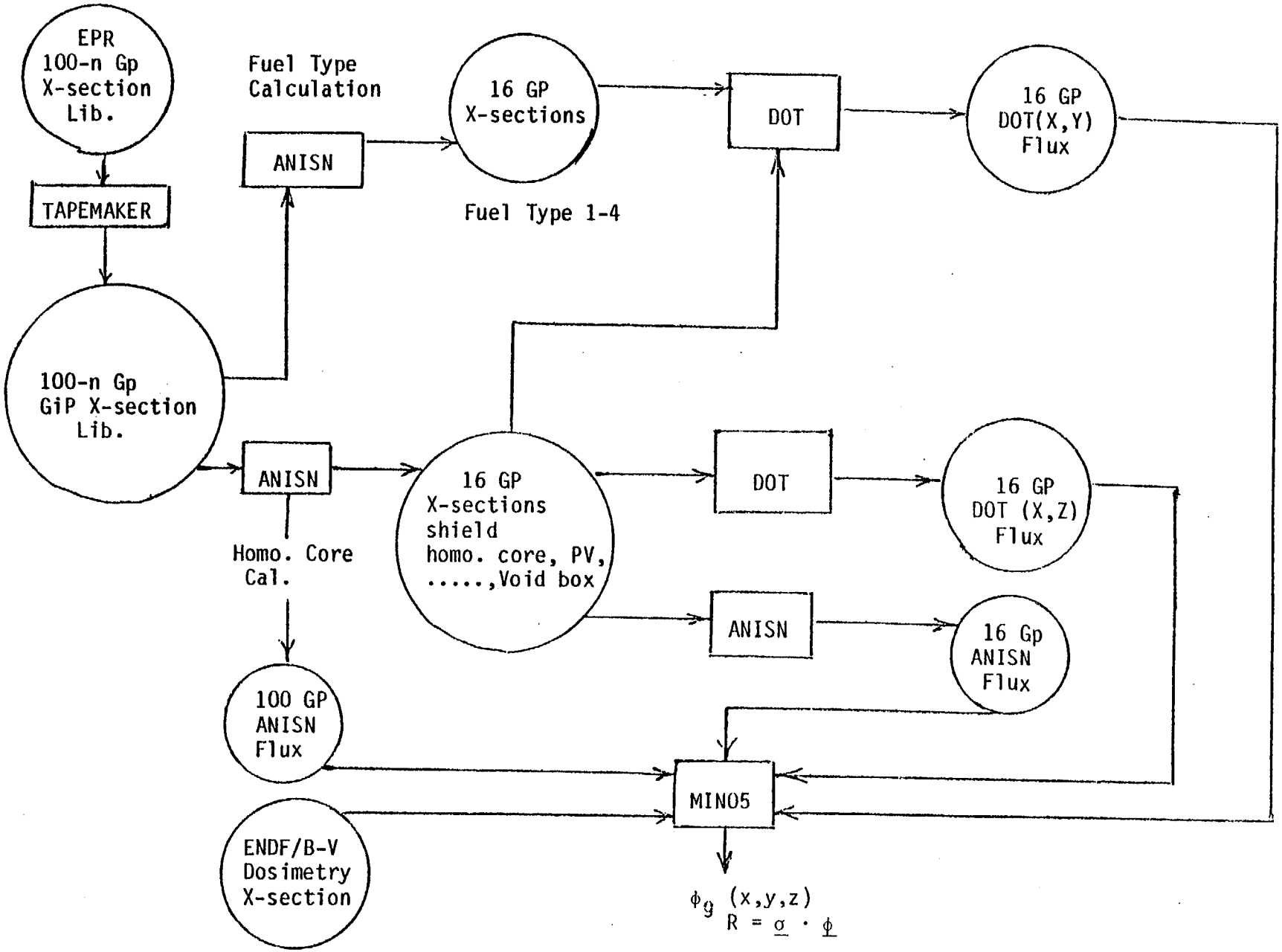

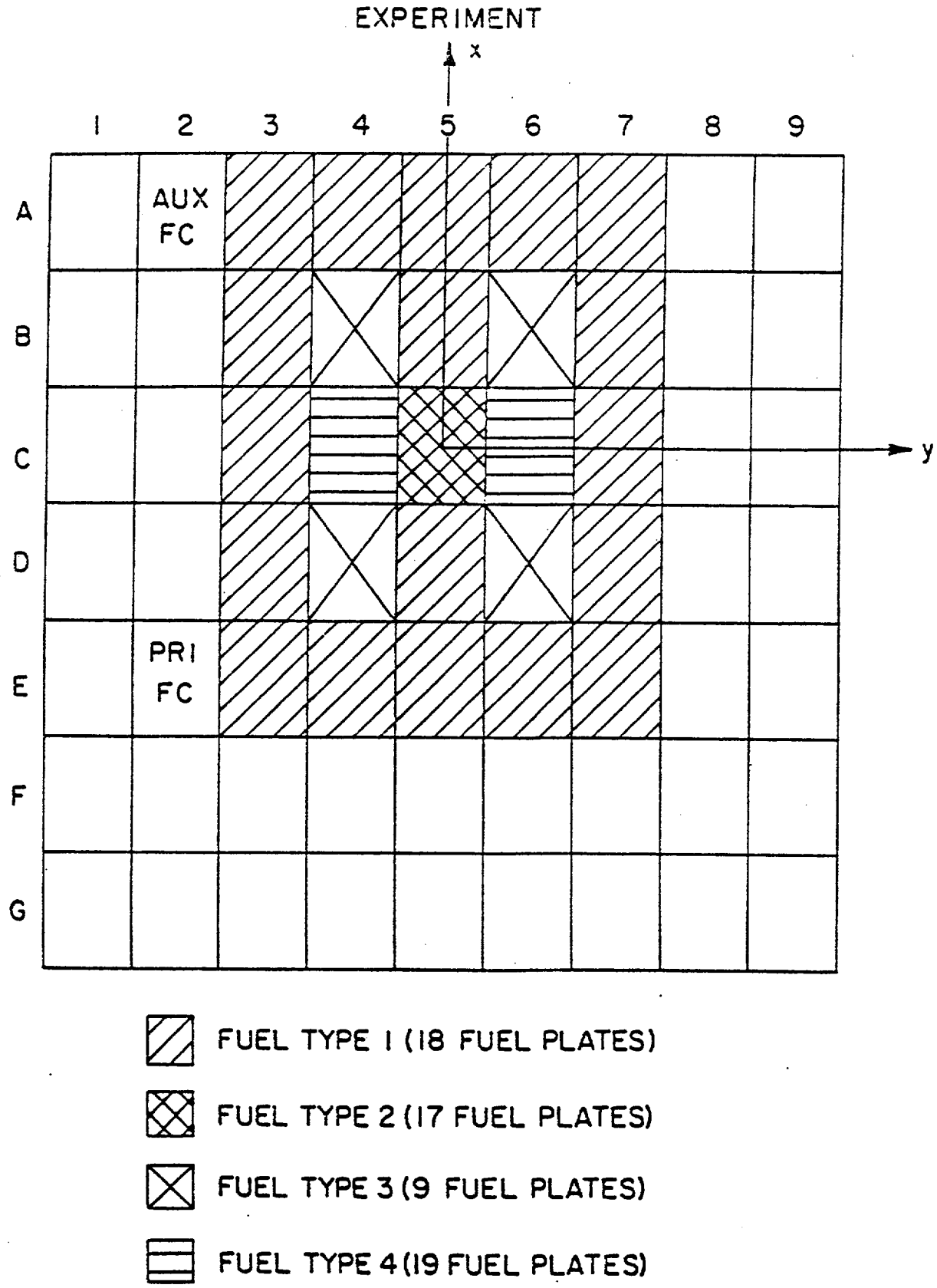

Figure 2. PCA Fuel Loading Pattern

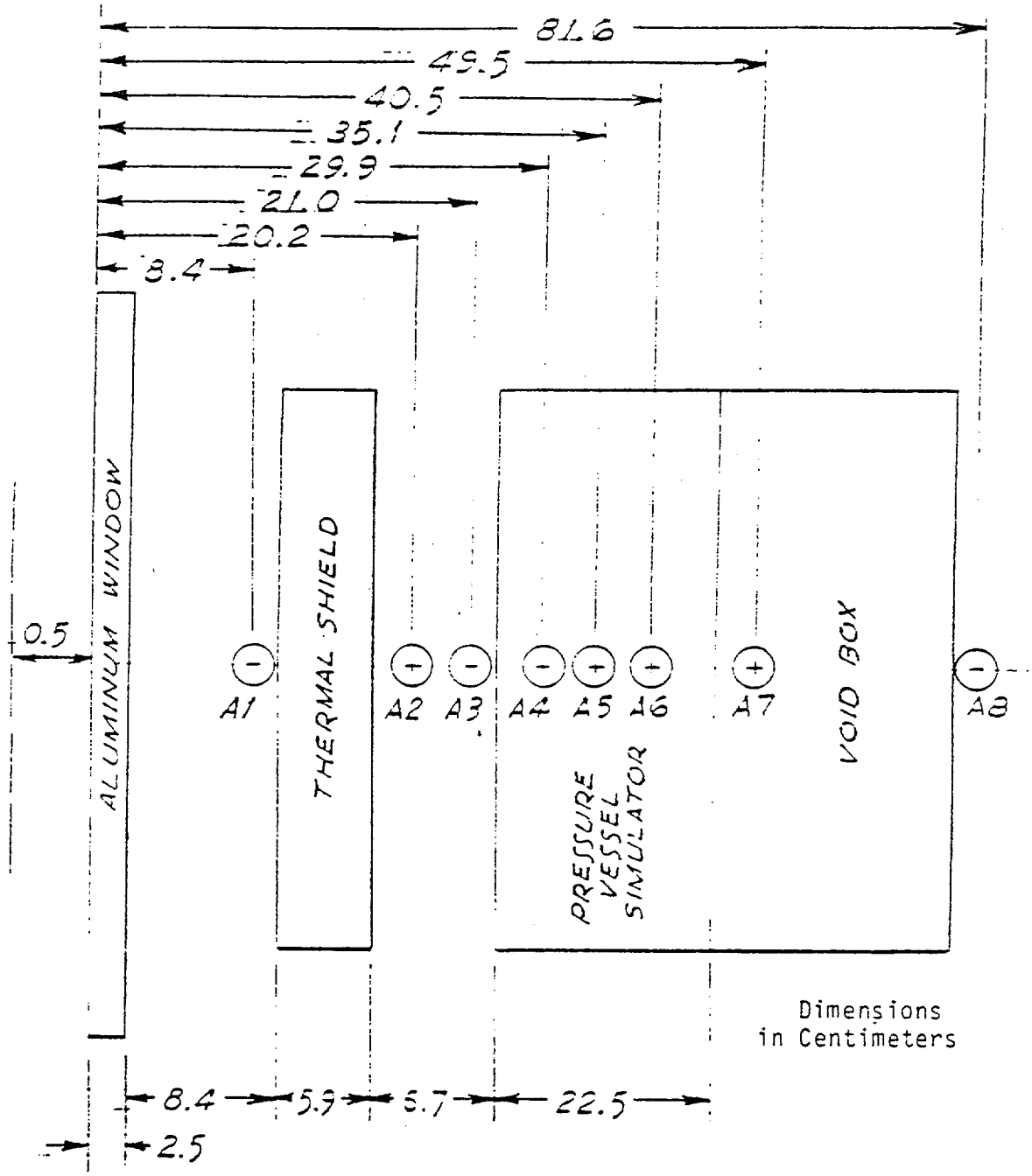

Measuring accuracy and reproducibility: ± 0.1 cm (2 sigma, estimated).

Deviations from exact geometry (surface imperfections, tilts): ± 0.2 cm maximum.

Figure 3. Detector Locations of PCA 8/7 Configuration

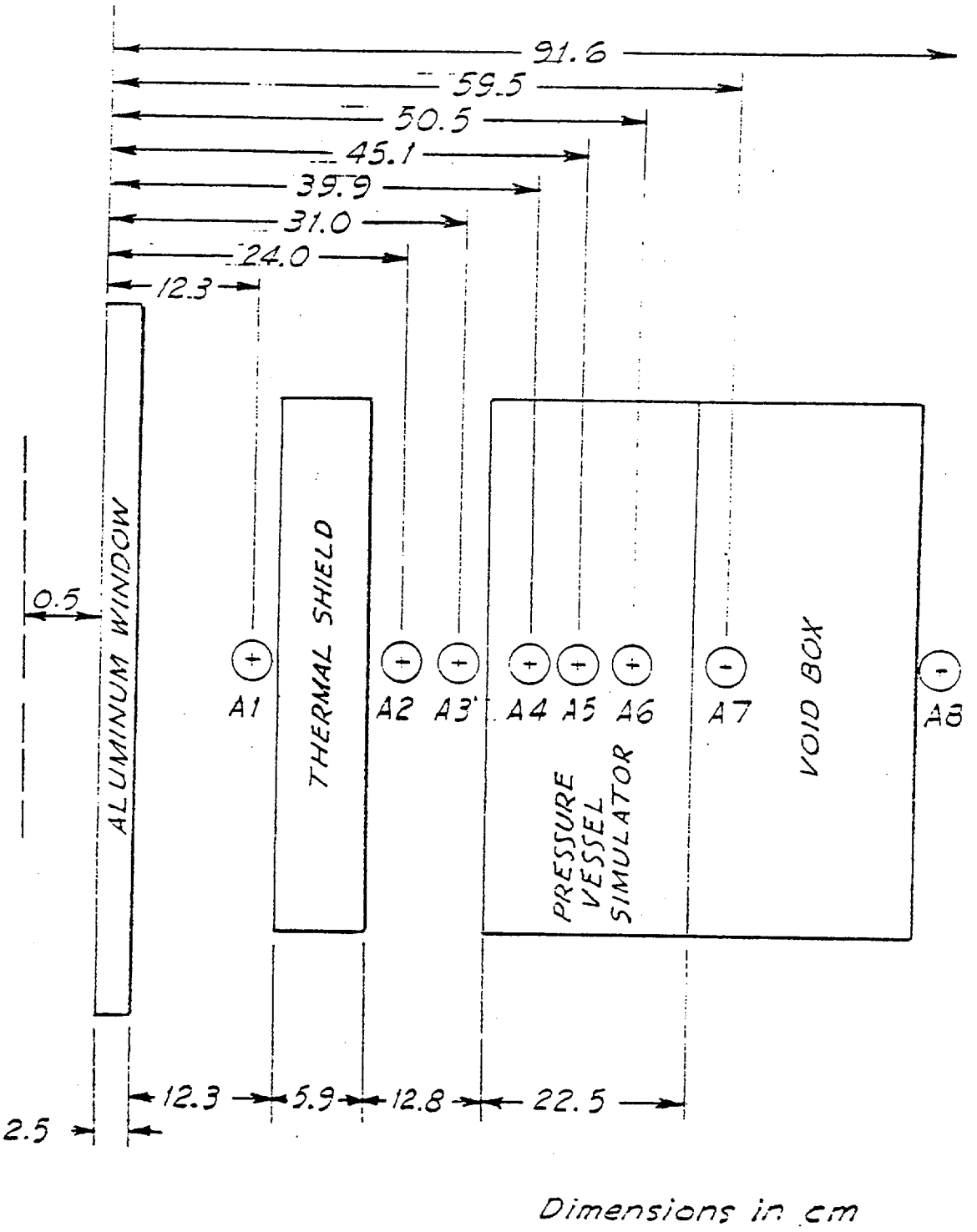

Figure 4. Detector Locations of PCA 12/13 Configuration

ZONE NO. 1 : FUEL TYPE 1 (18 PLATES)
2 : FUEL TYPE 2 (17 PLATES)
3 : FUEL TYPE 3 (9 PLATES)
4 : FUEL TYPE 4 (19 PLATES)
5 : WATER
6 : AL-WINDOW
7 : WATER
8 : THERMAL SHIELD (SS-304L)
9 : WATER
10 : PRESSURE VESSEL (C-STEEL)
11 : AL-WALL
12 : VOID BOX (AIR)
13 : AL-WALL
14 : WATER

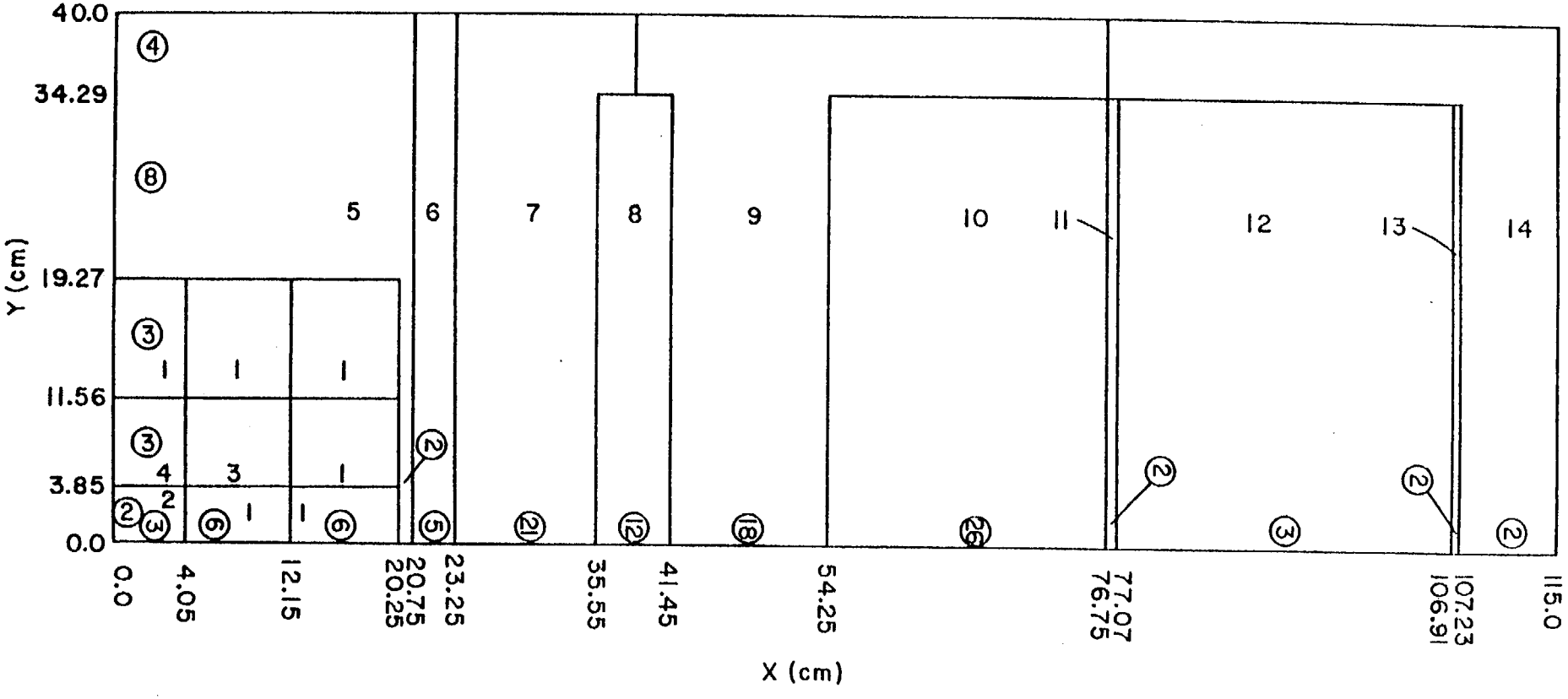

Figure 5. DOT (x,y) Model for the PCA 12/13 Configuration

ZONE NO. 1 : FUEL TYPE 1 (18 PLATES)
2 : FUEL TYPE 2 (17 PLATES)
3 : FUEL TYPE 3 (9 PLATES)
4 : FUEL TYPE 4 (19 PLATES)
5 : WATER
6 : AL-WINDOW
7 : WATER
8 : THERMAL SHIELD (SS-304L)
9 : WATER
10 : PRESSURE VESSEL (C-STEEL)
11 : AL-WALL
12 : VOID BOX (AIR)
13 : AL-WALL
14 : WATER

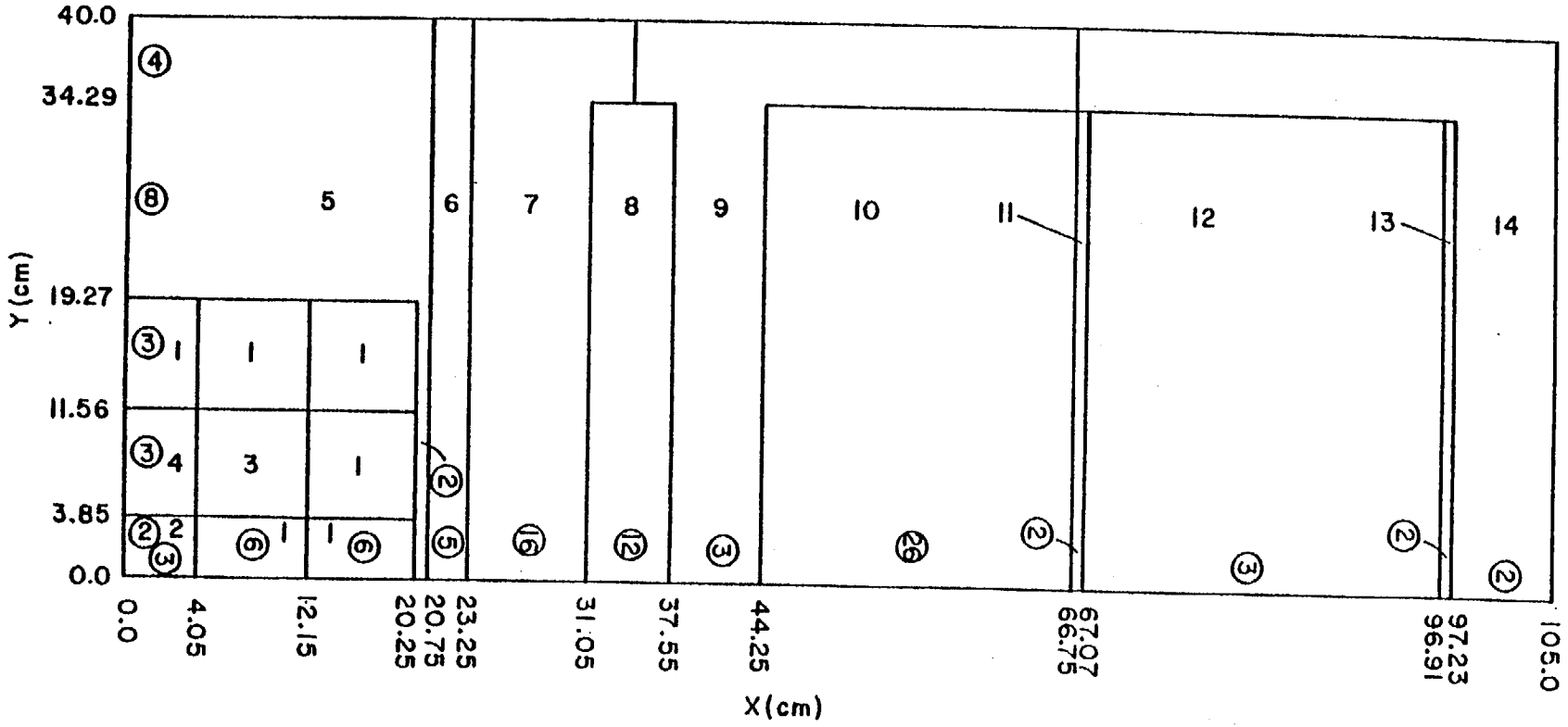

Figure 6. DOT (x,y) Model for the PCA 8/7 Configuration

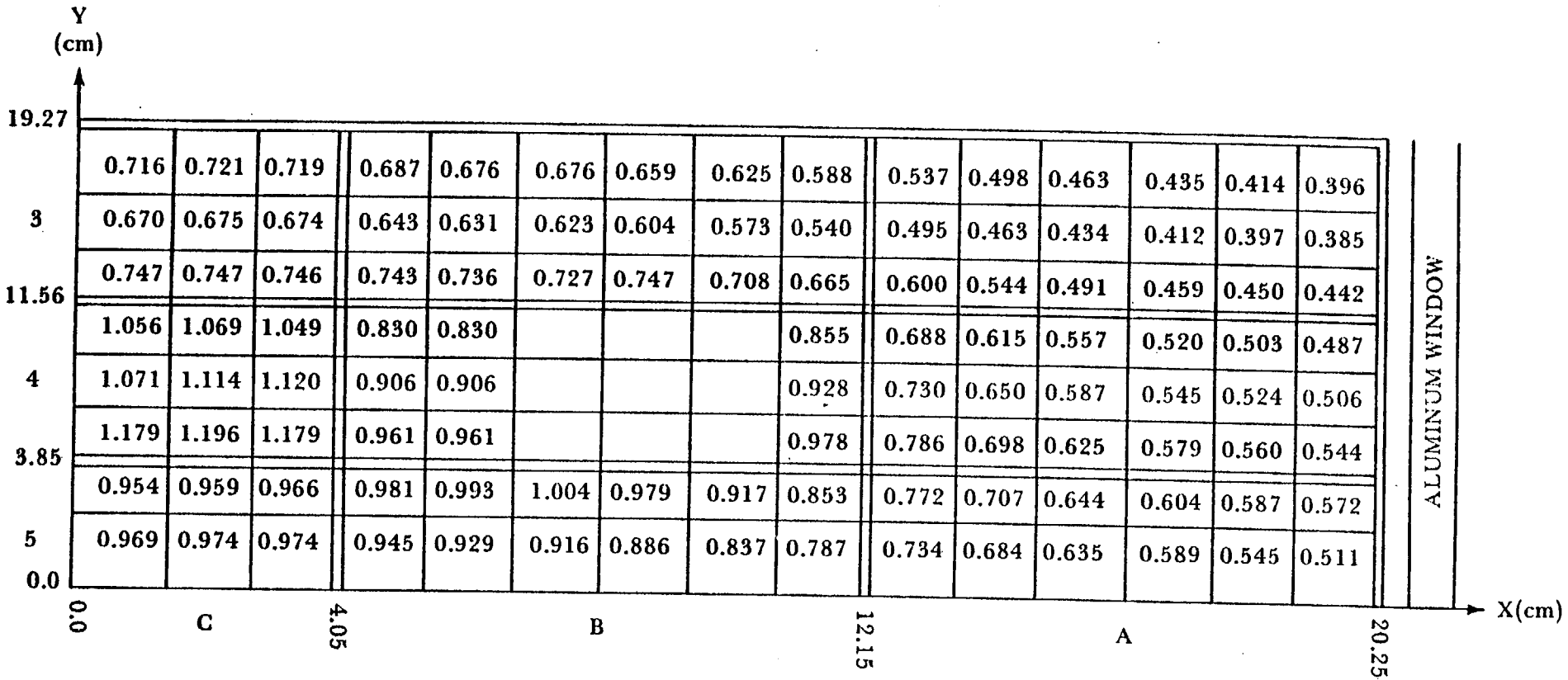

Figure 7. DOT (x,y) Model Power Distribution

ZONE NO. 1: CORE (HOMOGENIZED)
2: WATER
3: AL-WINDOW
4: WATER
5: THERMAL SHIELD (SS-304L)
7: PRESSURE VESSEL (C-STEEL)
8: AL-WALL
9: VOID BOX (AIR)
10: AL-WALL
11: WATER

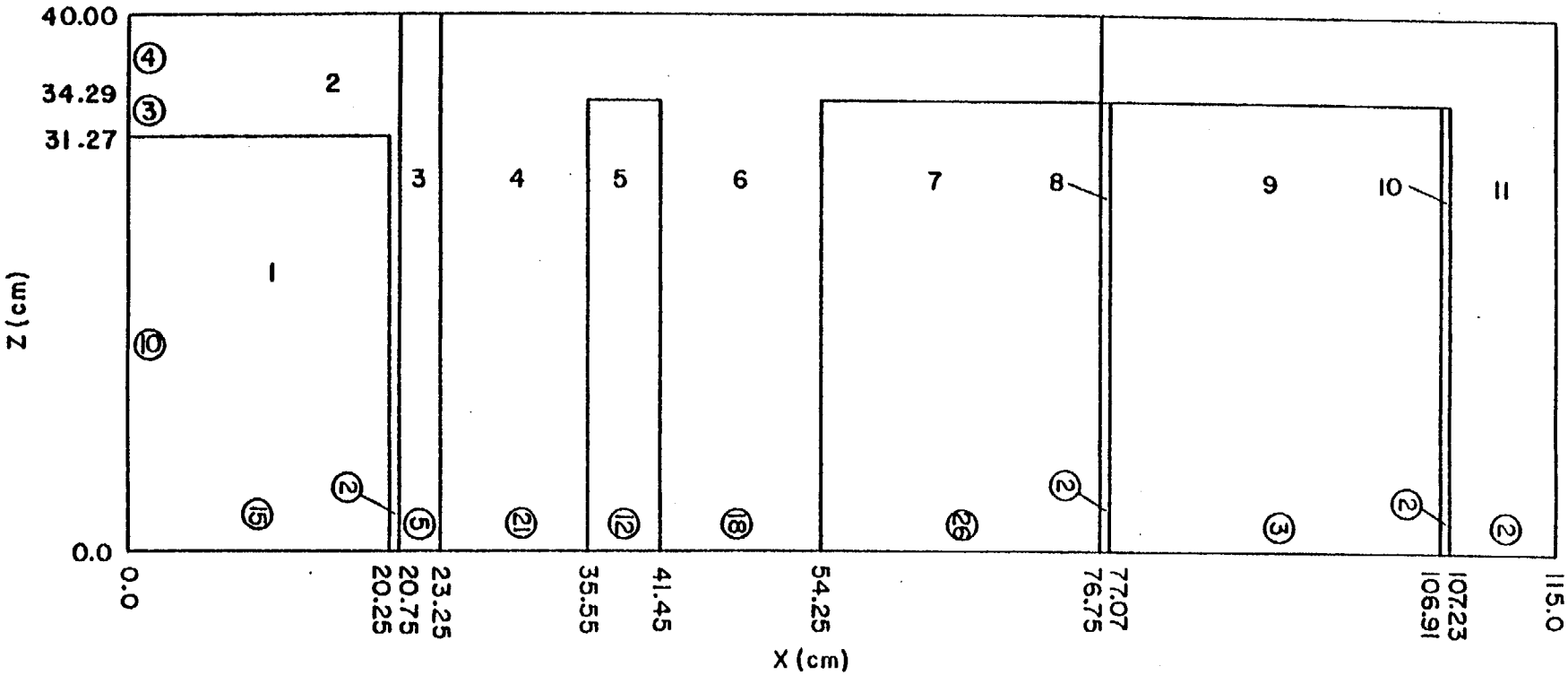

Figure 8. DOT (x,z) Model for the Axial Correction Factor Calculation (PCA 12/13 Configuration)

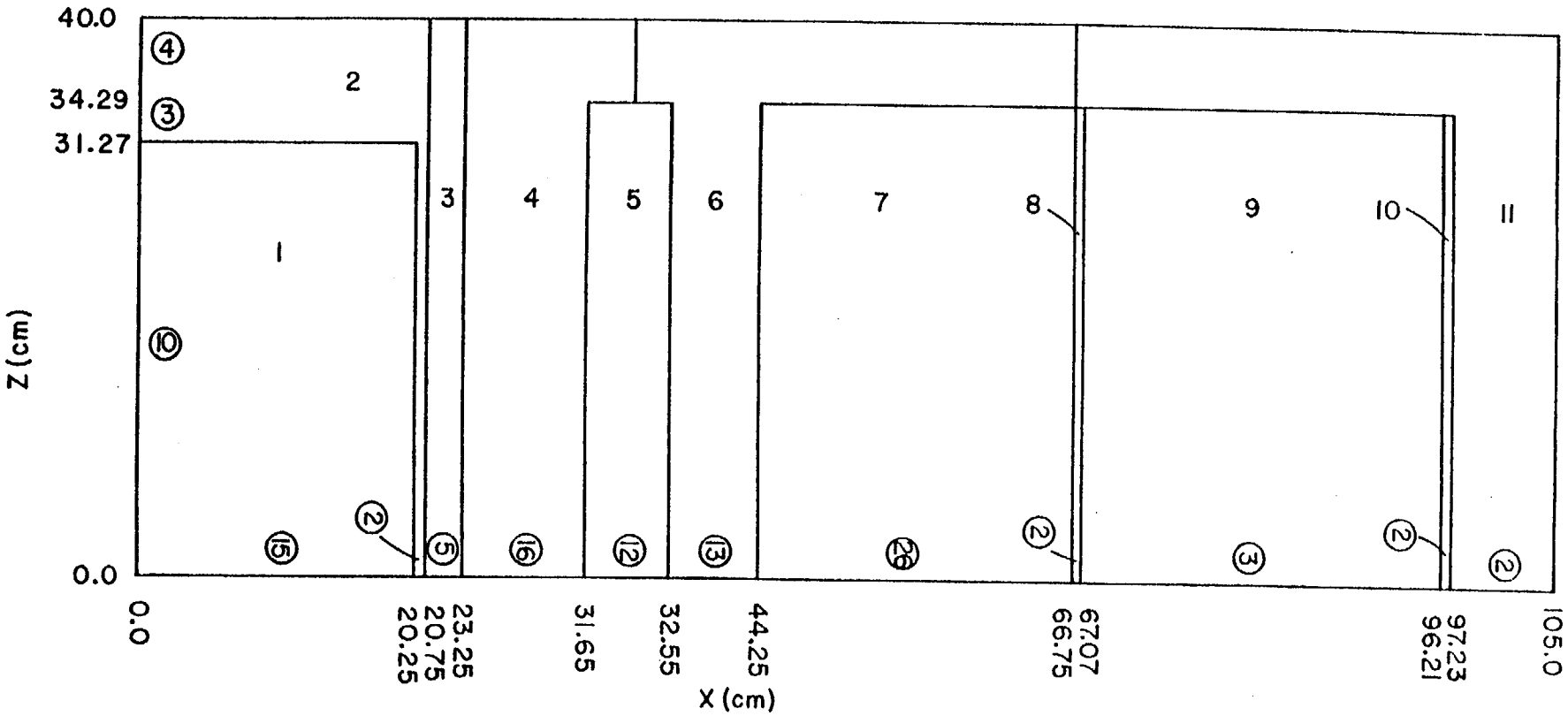

Figure 9. DOT (x,z) Model for the Axial Correction Factor Calculation (PCA 8/7 Configuration)

DISTRIBUTION LIST

U.S. Nuclear Regulatory Commission
- H. Denton
- W. Dircks
- M. Dunenfeld (2)
- D. Fieno (7)
- W. Hazelton
- W. Johnston
- P. Kapo
- L. Lois
- R. Minogue
- B. Morris
- T. Murley
- D. Ross
- L. Rubenstein
- C. Z. Serpan
- L. Tong

Public Document Room
Bethesda Technical Library
Advisory Committee Reactor Safeguards (16)

Brookhaven National Laboratory
- J. Carew
- W. Y. Kato

Core Performance Group
DNE Associate Chairmen
Nuclear Safety Group Leaders

Babcock & Wilcox
- J. Taylor
- C. Whitmarsh

Bechtel Power Company
- W. C. Hopkins

CEN/SCK
- G. DeLeeuw-Gierts
- S. DeLeeuw
- A. Fabry
- G. Minsart

Combustion Engineering, Inc.
- G. Cavanaugh
- R. Mills
- D. Stephens

EG&G Idaho
- J. W. Rogers

Exxon Nuclear Company, Inc.
- C. Owsley

Electric Power Research Institute
- B. Sehgal
- H. Till
- B. Zolotar

General Electric
- G. Sherwood

Hanford Engineering Development
- R. Gold
- G. Guthrie
- L. S. Kellogg
- E. P. Lippincott
- W. N. McElroy
- F. H. Ruddy

National Bureau of Standards
- C. Eisenhauer
- J. A. Grundl
- E. D. McGarry

Oak Ridge National Laboratory
- F.B.K. Kam
- R. E. Maerker
- L. F. Miller
- F. W. Stallmann

Southwest Research Institute
- E. B. Norris

Westinghouse Electric Corporation
- S. L. Anderson
- T. Anderson